JOURNAL OF COMPUTATIONAL PHYSICS **130,** 41–53 (1997)
ARTICLE NO. CP965442

A GMRES-Based Plane Smoother in Multigrid to Solve 3D Anisotropic Fluid Flow Problems*

C. W. Oosterlee

German National Research Center for Information Technology (GMD), Institute for Algorithms and Scientific Computing (SCAI), Schloss Birlinghoven, 53754 Sankt Augustin, Germany

Received May 10, 1995; revised December 8, 1995

For a discretization of the 3D steady incompressible Navier–Stokes equations a solution method is presented for solving flow problems on stretched grids. The discretization is a vertex-centered finite volume discretization with a flux splitting approach for the convective terms. Second-order accuracy is obtained with the well-known defect correction technique (B. Koren, *J. Comput. Phys.* **87,** 25, 1990). The solution method used is multigrid, for which a plane smoother is presented for obtaining good convergence in flow domains with severely stretched grids. A matrix is set up in a plane, which is solved iteratively with a preconditioned GMRES method. Here, a stop criterion for GMRES is tested, which reduces the number of inner iterations compared to an ''exact'' plane solver without affecting the multigrid convergence rates. The performance of the solution method is shown for a Poisson model problem and for 3D incompressible channel flow examples.

1. INTRODUCTION

With the appearance of supercomputers in the field of numerical mathematics, fast multigrid and preconditioned Krylov subspace solution methods were constructed for solving large systems of discretized partial differential equations. In the eighties the multigrid method became a very popular method for solving computational fluid dynamics problems. Its efficiency in solving nonlinear problems, for example in compressible Euler, Navier–Stokes, and incompressible Navier–Stokes equations, has led to many multigrid publications, mostly for block-structured applications. The fact that in nonlinear multigrid it is not necessary to store a matrix resulted in algorithms to solve very large (3D) systems of equations. An overview of multigrid solution methods for computational fluid dynamics problems is given in [35] and for incompressible Navier–Stokes equations also in [16].

Preconditioned Krylov subspace methods became very popular after the introduction of CGS [29] and GMRES [27]. It was then possible to solve nonsymmetric sparse matrices efficiently. An advantage of Krylov subspace methods is that linear systems are solved with a given matrix, which means that systems of equations can be solved by this black-box solver. More recently these methods are also being used for computational fluid dynamics problems, for block-structured grids for example in [34, 8]. Moreover, Krylov methods are very interesting for discretizations on unstructured grids, where robust multigrid smoothers from structured grids, like line smoothers, are often not available. A combination of both solution methods is not very often seen. Multigrid is sometimes used as preconditioner for Krylov methods [22], or as inner iteration in GMRES-type methods [38]. Here, we will combine both solution techniques for 3D incompressible fluid flow problems with severe stretching of grid cells.

Several methods have been proposed for the discretization of steady incompressible Navier–Stokes equations on block-structured grids. Probably the most widely adopted approach is to use Cartesian velocity unknowns and pressure as dependent variables on a collocated grid. The pioneering papers of this collocated approach are by Rhie and Chow [24] and Peric [20]. In our work the collocated approach is also adopted for solving the steady equations. The 3D equations are discretized on a block-structured grid with vertex-centered finite volumes. The discretization in general domains is presented in [18] and is based on the 2D discretization in [7]. With a flux splitting formulation of the steady incompressible Navier–Stokes equations, well-known discretization and solution methods derived from steady compressible Navier–Stokes equations can be used, such as in [13]. A first-order accurate upwind discretization with polynomial flux difference splitting for the convective terms [7] is implemented for solving the steady equations directly. Second-order accuracy is obtained with van Leer's second-order κ-scheme [33] in the defect correction technique. Nonlinear multigrid (FAS) is used as inner iteration in defect correction (see [13, 35]).

It is well known that for the Poisson equation the convergence rate of standard multigrid with a point smoother tends to one for anisotropic problems, when anisotropies get more pronounced. Anisotropies might for example oc-

* This work was supported by the German Federal Ministry for Research and Education under Contract IR302A7 (POPINDA Project).

0021-9991/97 $25.00

cur as result of a severe stretching of grid cells. For certain types of stretching of 3D grid cells a plane smoother is a necessary requirement for satisfactory standard multigrid convergence [30]. Also in [3] a plane smoother was used. There it was based on ILU relaxation for solving a 3D Poisson equation. In the present work, plane Gauss–Seidel smoothers which visit planes in lexicographical and zebra-type ordering are implemented and evaluated. All unknowns in a plane are updated simultaneously; a 2D matrix is set up, which is solved iteratively with a preconditioned GMRES [27] method. A stop criterion for the GMRES plane solver is evaluated, which reduces the number of inner iterations compared to an "exact" plane solver drastically, without influencing the multigrid convergence. Firstly, this algorithm is tested for the 3D Poisson equation on stretched grids.

For discretizations of 3D steady incompressible Navier–Stokes equations on a stretched grid it is not clear a priori when a plane smoother is a necessary requirement, if all equations are smoothed simultaneously. The coupled set of equations consists of three nonlinear momentum equations, for which the main classification depends on the Reynolds number, and the continuity equation, whose discretization often results in an additional Poisson term for the pressure. The multigrid algorithms with line and plane smoother are compared for channel flow problems at different Reynolds numbers with grid stretching in length direction.

The discretization and solution method are set up in a parallel multiblock environment. With grid partitioning [14] different blocks are solved in parallel on different processors of a MIMD machine. The communication among the nodes on all multigrid levels is handled by a high-level communications library CLIC [26], based on the portable message-passing interface PARMACS [6]. Finally, a multiblock 3D backward-facing step problem is solved, in which a 3D grid is generated with different grid stretching in the three directions.

2. DISCRETIZATION OF INCOMPRESSIBLE NAVIER–STOKES EQUATIONS

In Cartesian coordinates the steady incompressible Navier–Stokes equations are written as a system of equations as

$$\frac{\partial \mathbf{f}}{\partial x}+\frac{\partial \mathbf{g}}{\partial y}+\frac{\partial \mathbf{h}}{\partial z}=\frac{\partial \mathbf{f_v}}{\partial x}+\frac{\partial \mathbf{g_v}}{\partial y}+\frac{\partial \mathbf{h_v}}{\partial z}, \tag{1}$$

where $\mathbf{f}$, $\mathbf{g}$, $\mathbf{h}$ are the components of the convective flux vector, and $\mathbf{f_v}$, $\mathbf{g_v}$, and $\mathbf{h_v}$ are the viscous fluxes:

$$\mathbf{f}=\begin{bmatrix} u^2+p \\ uv \\ uw \\ c^2u \end{bmatrix},\quad \mathbf{g}=\begin{bmatrix} uv \\ v^2+p \\ vw \\ c^2v \end{bmatrix},\quad \mathbf{h}=\begin{bmatrix} uw \\ vw \\ w^2+p \\ c^2w \end{bmatrix}$$

$$\mathbf{f_v}=\begin{bmatrix} \frac{1}{\mathrm{Re}}\,\partial u/\partial x \\ \frac{1}{\mathrm{Re}}\,\partial v/\partial x \\ \frac{1}{\mathrm{Re}}\,\partial w/\partial x \\ 0 \end{bmatrix},\quad \mathbf{g_v}=\begin{bmatrix} \frac{1}{\mathrm{Re}}\,\partial u/\partial y \\ \frac{1}{\mathrm{Re}}\,\partial v/\partial y \\ \frac{1}{\mathrm{Re}}\,\partial w/\partial y \\ 0 \end{bmatrix},$$

$$\mathbf{h_v}=\begin{bmatrix} \frac{1}{\mathrm{Re}}\,\partial u/\partial z \\ \frac{1}{\mathrm{Re}}\,\partial v/\partial z \\ \frac{1}{\mathrm{Re}}\,\partial w/\partial z \\ 0 \end{bmatrix}.$$

Here u, v, and w are Cartesian velocity unknowns, p is pressure, c is a constant reference velocity, and Re is the Reynolds number defined as: $\mathrm{Re}=\overline{U}\cdot L/\nu$, with $\overline{U}$ a characteristic velocity, L a characteristic length and ν the kinematic viscosity.

Differences of the convective fluxes with respect to $\mathbf{u}$ can be written as

$$\Delta\mathbf{f}=A_1\Delta\mathbf{u},\quad \Delta\mathbf{g}=A_2\Delta\mathbf{u},\quad \Delta\mathbf{h}=A_3\Delta\mathbf{u} \tag{2}$$

with $\mathbf{u}=(u, v, w, p)^{\mathrm{T}}$ and A_1, A_2, and A_3 are the discrete Jacobians,

$$A_1=\begin{bmatrix} 2\overline{u} & 0 & 0 & 1 \\ \overline{v} & \overline{u} & 0 & 0 \\ \overline{w} & 0 & \overline{u} & 0 \\ c^2 & 0 & 0 & 0 \end{bmatrix},\quad A_2=\begin{bmatrix} \overline{v} & \overline{u} & 0 & 0 \\ 0 & 2\overline{v} & 0 & 1 \\ 0 & \overline{w} & \overline{v} & 0 \\ 0 & c^2 & 0 & 0 \end{bmatrix},$$

$$A_3=\begin{bmatrix} \overline{w} & 0 & \overline{u} & 0 \\ 0 & \overline{w} & \overline{v} & 0 \\ 0 & 0 & 2\overline{w} & 1 \\ 0 & 0 & c^2 & 0 \end{bmatrix},$$

where the overbar denotes the mean of variables: $u=\overline{u}+\Delta u$, $(\overline{u}_{i+1/2,j,k}=\frac{1}{2}(u_{i,j,k}+u_{i+1,j,k})$, etc.).

Matrix A will be written as a combination of A_1, A_2, and A_3 as

$$A = n_x A_1 + n_y A_2 + n_z A_3 = \begin{bmatrix} n_x\overline{u} + r & n_y\overline{u} & n_z\overline{u} & n_x \\ n_x\overline{v} & n_y\overline{v} + r & n_z\overline{v} & n_y \\ n_x\overline{w} & n_y\overline{w} & n_z\overline{w} + r & n_z \\ n_x c^2 & n_y c^2 & n_z c^2 & 0 \end{bmatrix}. \tag{3}$$

Here $r = n_x\overline{u} + n_y\overline{v} + n_z\overline{w}$, and (n_x, n_y, n_z) are components of a normal vector. Using $n_x^2 + n_y^2 + n_z^2 = 1$, a set of three different eigenvectors is found for matrix A: $\lambda_1 = \lambda_2 = r$, $\lambda_3 = r + a$, $\lambda_4 = r - a$, with $a = \sqrt{r^2 + c^2}$.

However, a full set of four left and right eigenvectors was found. With left and right eigenvector matrices L and R matrix A will be split into negative and positive parts A^- and A^+,

$$A^- = R\Lambda^- L, \quad A^+ = R\Lambda^+ L, \quad A = A^- + A^+, \tag{4}$$

$\Lambda^- = \lambda^- I$, $\Lambda^+ = \lambda^+ I$, $\lambda_i^- = \min(\lambda_i, 0)$, $\lambda_i^+ = \max(\lambda_i, 0)$, $i = 1, 4$. (I is the identity matrix.)

The resulting formula for the finite volume discretization is found with (3) and (4); a linear combination of flux differences can be expressed as

$$n_x\Delta\mathbf{f} + n_y\Delta\mathbf{g} + n_z\Delta\mathbf{h} = (A^- + A^+)\,\Delta\mathbf{u}. \tag{5}$$

The 3D vertex-centered finite volume discretization of (1) in general domains is presented in [18] and is based on the 2D discretization in [7]. In the present work mainly problems in Cartesian domains will be considered. The most important aspects of the finite volume discretization are repeated briefly. Integration of the convective part of (1) over a control volume $\Omega_{i,j,k}$ gives

$$\int_{\Omega_{i,j,k}} \left(\frac{\partial\mathbf{f}}{\partial x} + \frac{\partial\mathbf{g}}{\partial y} + \frac{\partial\mathbf{h}}{\partial z}\right) \partial\Omega = F.dS\big|_{i-1/2,j,k}^{i+1/2,j,k} + F.dS\big|_{i,j-1/2,k}^{i,j+1/2,k} + F.dS\big|_{i,j,k-1/2}^{i,j,k+1/2}, \tag{6}$$

where $F = \mathbf{n}.\mathbf{F}$ with $\mathbf{F} = (\mathbf{f}, \mathbf{g}, \mathbf{h})^{\mathrm{T}}$, $\mathbf{n} = (n_x, n_y, n_z)^{\mathrm{T}}$ is the outward normal vector on the volume side, and dS the length of the volume side.

As an example, the evaluation of flux $F_{i+1/2,j,k}$ in (6) is shown. For $F_{i+1/2,j,k}$ an upwind definition is used,

$$F_{i+1/2,j,k} = 1/2(F_{i,j,k} + F_{i+1,j,k} - |\Delta F_{i,i+1}|), \tag{7}$$

$\Delta F_{i,i+1}$ is found with (2) and (3),

$$F_{i,i+1} = F_{i+1,j,k} - F_{i,j,k} = A_{i,i+1}\,\Delta\mathbf{u}_{i,i+1}, \tag{8}$$

where $A_{i,i+1}$ is built as in (3) with $\overline{\mathbf{u}}$-values coming from $(i, j, k)^{\mathrm{T}}$ and $(i + 1, j, k)^{\mathrm{T}}$, and $\Delta\mathbf{u}_{i,i+1} = \mathbf{u}_{i+1,j,k} - \mathbf{u}_{i,j,k}$. With (4) for the absolute value of $\Delta F_{i,i+1}$ is found,

$$|\Delta F_{i,i+1}| = (A_{i,i+1}^+ - A_{i,i+1}^-)\,\Delta\mathbf{u}_{i,i+1}. \tag{9}$$

The formula used in the discretization follows from (5), (7), and (8),

$$\begin{aligned} F_{i+1/2,j,k} &= F_{i,j,k} + 1/2(F_{i+1,j,k} - F_{i,j,k}) - 1/2|\Delta F_{i,i+1}| \\ &= F_{i,j,k} + 1/2A_{i,i+1}\,\Delta\mathbf{u}_{i,i+1} - 1/2|\Delta F_{i,i+1}| \\ &= F_{i,j,k} + A_{i,i+1}^-\,\Delta\mathbf{u}_{i,i+1}. \end{aligned} \tag{10}$$

The fluxes on the other volume boundaries in (6) are treated in the same way.

The viscous fluxes $\mathbf{f_v}$, $\mathbf{g_v}$, and $\mathbf{h_v}$ are discretized with the Peyret control volume technique [21]. Second derivatives disappear with a shifted control volume [21, 7].

The treatment of boundary conditions, which is described in detail in [7] is generalized to three dimensions in [18]. The resulting discretization is first-order accurate and is so-called positive; the resulting matrix is a K-matrix [35]. Irreducible K-matrices lead to M-matrices [35], which are favorable for iterative solution. With defect correction [13, 35] second-order accuracy can be obtained by iterating with a first-order discretized operator. The right-hand side is then corrected with a second-order operator. For defect correction techniques within multigrid a common approach is that only on the finest grid the right-hand side is corrected. The second-order scheme used in defect correction is van Leer's κ-scheme [33]. The vectors $\mathbf{u}_{i,j,k}$ and $\mathbf{u}_{i+1,j,k}$ in (7) and (8) are replaced by respectively,

$$\begin{aligned} \mathbf{u}_{i,j,k} &\leftarrow \mathbf{u}_{i,j,k} + \frac{1+\kappa}{4}(\mathbf{u}_{i-1,j,k} - \mathbf{u}_{i,j,k}) + \frac{1-\kappa}{4}(\mathbf{u}_{i,j,k} - \mathbf{u}_{i+1,j,k}) \\ \mathbf{u}_{i+1,j,k} &\leftarrow \mathbf{u}_{i+1,j,k} + \frac{1+\kappa}{4}(\mathbf{u}_{i,j,k} - \mathbf{u}_{i+1,j,k}) + \frac{1-\kappa}{4}(\mathbf{u}_{i+1,j,k} - \mathbf{u}_{i+2,j,k}). \end{aligned} \tag{11}$$

In the y- and z-direction vectors $\mathbf{u}_{i,j,k}$, $\mathbf{u}_{i,j\pm1,k}$, $\mathbf{u}_{i,j,k\pm1}$ are replaced in a similar way.

All tests have been made with $\kappa = 0$, the Fromm scheme. For incompressible Navier–Stokes equations it is not necessary to implement a limiter. For many (2D and 3D) different problems at low and high Reynolds numbers wiggles, oscillations (for example, in the pressure distribution, as they occur near discontinuities for compressible flow problems), did not appear. Discontinuities in the pressure distribution do not occur.

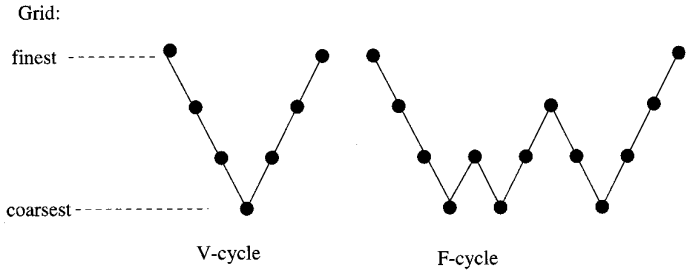

FIG. 1. The multigrid F and F cycling strategies.

3. THE PARALLEL MULTIGRID METHOD

The parallel multigrid algorithm consists of a host and a node program. The host program creates node processes, sends initial data to the nodes, and receives calculated results. Each node program performs the calculations and communicates with other nodes. The parallelization is done with the 3D block-structured communications library CLIC, developed at GMD [26]. CLIC provides subroutines for all communication tasks occurring in multiblock multigrid applications. Its portability is assured by an implementation using the message passing interface PARMACS [6]. CLIC is also used for the parallelization of industrial aerodynamics codes [9]. The parallelization technique used to distribute parts of a domain to different processes is grid partitioning [14]. The domain is split into blocks. Along the interior block boundaries an overlap region is defined, and all operations in multigrid are performed in parallel.

Standard nonlinear multigrid (FAS) is employed, consisting of 3D restriction and prolongation operators, a coarse grid operator coming from a direct discretization of the partial differential equations on the coarse grid and several Gauss–Seidel type smoothing methods. Next to the multigrid V-cycle, also the F-cycle is used here. Figure 1 shows the cycling strategy of a V- and an F-cycle.

Transfer Operators. The restricted fine grid approximate solution is only a starting approximation on a coarse grid in the FAS algorithm; therefore a simple restriction operator is sufficient. For this purpose an injection operator is chosen. A part of the coarse grid right-hand side, $f_{I,J,K}$, is a full weighting restriction of fine grid residuals, r:

$$\begin{aligned} f_{I,J,K} = {} & \tfrac{1}{8} r_{2i-1,2j-1,2k-1} \\ & + \tfrac{1}{16}(r_{2i-2,2j-1,2k-1} + r_{2i,2j-1,2k-1} + r_{2i-1,2j-2,2k-1} + r_{2i-1,2j,2k-1} \\ & + r_{2i-1,2j-1,2k-2} + r_{2i-1,2j-1,2k}) \\ & + \tfrac{1}{32}(r_{2i-2,2j-2,2k-1} + r_{2i-2,2j-1,2k-2} + r_{2i-1,2j-2,2k-2} + r_{2i,2j,2k-1} \\ & + r_{2i,2j-1,2k} + r_{2i-1,2j,2k} + r_{2i-2,2j,2k-1} \\ & + r_{2i-2,2j-1,2k} + r_{2i-1,2j-2,2k} + r_{2i-1,2j,2k-2} \\ & + r_{2i,2j-2,2k-1} + r_{2i,2j-1,2k-2}) \\ & + \tfrac{1}{64}(r_{2i-2,2j-2,2k-2} + r_{2i-2,2j-2,2k} + r_{2i-2,2j,2k-2} + r_{2i,2j-2,2k-2} \\ & + r_{2i,2j,2k} + r_{2i-2,2j,2k} + r_{2i,2j-2,2k} + r_{2i,2j,2k-2}). \end{aligned} \tag{12}$$

This contribution of different fine-grid residuals to the coarse-grid right-hand side is also depicted in Fig. 2. In CFD research it is not common to use transfer operators that depend on the operator. Full weighting for restriction operators is a standard choice in CFD problems that can be found, for example, in [35].

The prolongation operator prolongates corrections of unknowns to finer grids. Here, 3D trilinear interpolation is used.

Smoothing Method. The most important part of a standard multigrid method is the smoothing algorithm. Robustness depends in many cases primarily on the smoothing algorithm as does efficiency. Several types of Gauss–Seidel smoothing methods are implemented that update a system of coupled equations simultaneously, as advocated in [1]. For discretizations of incompressible Navier–Stokes equations on staggered grids, coupled smoothers are well known [32, 31, 16]. In the smoothing methods corrections, $\mathbf{u}'$, to the current solution, $\mathbf{u^n}$, are calculated. Thus,

$$\tilde{\mathbf{B}}(\mathbf{u}') = \mathbf{f} - \mathbf{B}(\mathbf{u^n}), \tag{13}$$

where $\tilde{\mathbf{B}}$ represents a smoothing operator.

These corrections are added to the current solution with underrelaxation factor ω,

$$\mathbf{u^{n+1}} = \mathbf{u^n} + \omega \mathbf{u}'. \tag{14}$$

Another type of smoothing methods for steady incom-

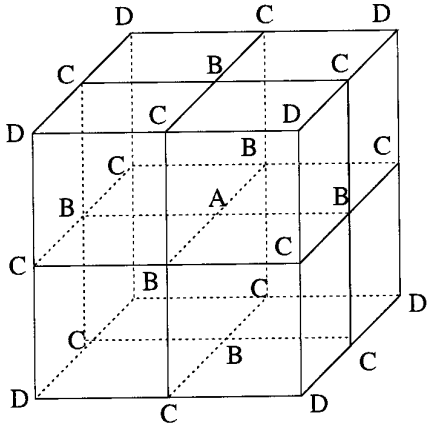

FIG. 2. The restriction contributions for the coarse grid vertex in the cube's center: point A: contribution with $\frac{1}{8}$, B: with $\frac{1}{16}$, C: with $\frac{1}{32}$, and D: with $\frac{1}{64}$.

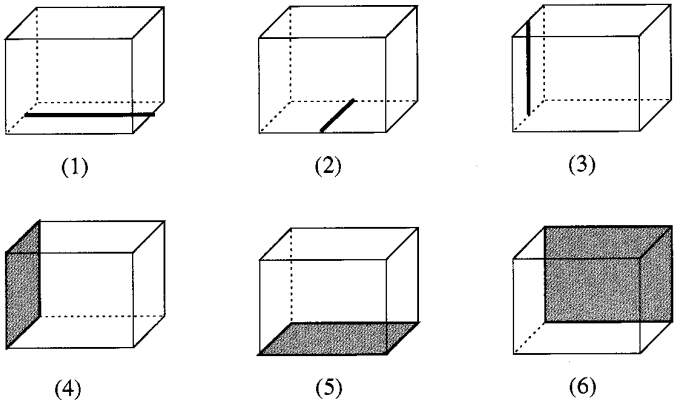

FIG. 3. An example of unknowns that are updated simultaneously in different smoothers for block-structured grids: (1) xLGS; (2) yLGS; (3) zLGS; (4) (y,z)GS; (5) (x,y)GS; (6) (x,z)GS.

pressible Navier–Stokes equations is the distributive smoother-type, where the different equations are updated uncoupled. Examples of distributive smoothers are SIMPLE [19, 23] pressure correction methods, distributive Gauss–Seidel [4], and distributive ILU smoothers [36, 37].

Implemented in our code are point coupled Gauss–Seidel smoothers, in which grid points are processed point-by-point, an x-line, y-line, and z-line coupled Gauss–Seidel smoother (xLGS, yLGS, and zLGS), and (x,y)-plane, (x,z)-plane, and (y,z)-plane Gauss–Seidel smoothers ((x,y)GS, (x,z)GS, (y,z)GS) that visit planes in lexicographical order. Moreover, zebra plane Gauss–Seidel smoothers ((x,y)ZGS etc.) are constructed that in a first stage visit all odd (white) planes and in a second stage visit all even (black) planes.

An x-line smoother updates unknowns on a line $y = \text{const.}$ and $z = \text{const.}$ An (x,y)-plane smoother updates all unknowns in an (x,y)-plane; see Fig. 3. All smoothers set up a matrix for all unknowns that are updated simultaneously. For point and line smoothers this matrix is solved directly with a band LU solver. For the plane smoothers the matrix is solved iteratively with a preconditioned GMRES solver [27]. The number of vectors for storing the Arnoldi basis is chosen as 35. The preconditioner is a truncated ILU decomposition, as presented in [28]. The drop tolerance is set to 10^{-2}. To the author's knowledge general black-box multigrid methods for solving matrices coming from systems of equations are not yet available.

In order to keep the plane smoother as cheap as possible the GMRES stop criterion ε is investigated. This is defined as $\sum_{i=1}^{ieq} (|r^{i(n)}|_2/|r^{i(0)}|_2)$, the 2-norm of the sum of residuals in the plane after n GMRES iterations divided by the 2-norm of the initial residual for ieq equations. For scalar partial differential equations $ieq = 1$, while for the 3D system of incompressible Navier–Stokes equations $ieq = 4$. The resulting criterion reduces the number of GMRES iterations considerably, compared to $\varepsilon = 10^{-8}$, which represents the fact that a plane is solved with high accuracy. It will be shown that it does not influence the multigrid convergence.

In the following section the smoothers are evaluated for test problems coming from the 3D Poisson equation and from 3D steady incompressible Navier–Stokes equations.

4. RESULTS

Average reduction factors, μ_n, are presented defined as

$$\mu_n = \left(\frac{\sum_{i=1}^{ieq} |r^{i(n)}|_\infty}{\sum_{i=1}^{ieq} |r^{i(0)}|_\infty} \right)^{1/n}. \tag{15}$$

This expression is very similar to the stop criterion for the GMRES iteration. The main difference is that here the maximum norm is being used in order to see the convergence of single largest residuals.

4.1. *Poisson Equation*

First, a Poisson equation on a 3D cubic domain is investigated,

$$\begin{aligned} \frac{\partial^2 \phi}{\partial x^2} + \frac{\partial^2 \phi}{\partial y^2} + \frac{\partial^2 \phi}{\partial z^2} &= 4 \quad \text{on } (0,1) \times (0,1) \\ \phi|_\Gamma &= 0. \end{aligned} \tag{16}$$

In [30] two-level analysis was performed and in [10] multigrid results were obtained with a lexicographical plane Gauss–Seidel smoother, in which 2D multigrid was used as plane solver. In [3] an ILU method was used as plane solver in 3D multigrid. We try to confirm the need for a plane smoother for the test cases from [30]. Multigrid convergence results are evaluated for the algorithms with an alternating line and a lexicographical plane smoother with different stop criteria. The 3D domain with length parameters L_1, L_2, and L_3 is shown in Fig. 4. The domain is discretized with an equal number of grid points in each direction. Parameters L_1, L_2, and L_3 are chosen such that

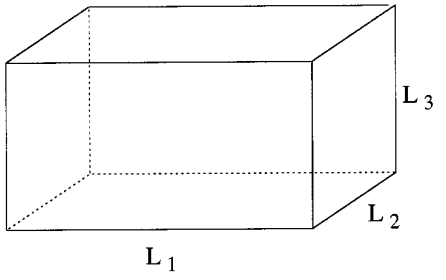

FIG. 4. The single block domain for the model test problems.

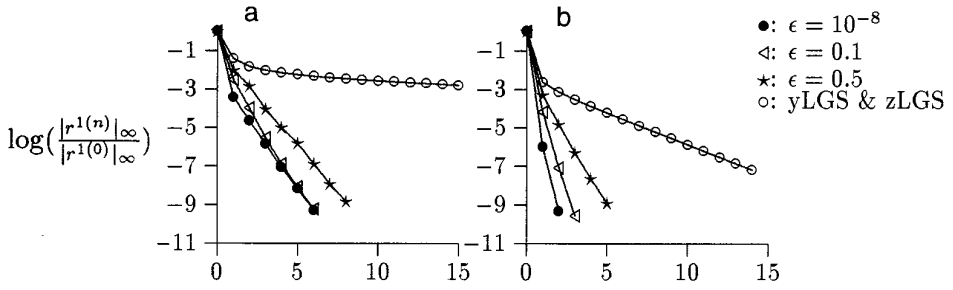

FIG. 5. V(1,1) multigrid convergence for 3D Poisson's equation (49^3-grid). A lexicographical (y,z)-plane smoother with different stop criteria for the GMRES plane solver is compared with an alternating line smoother (yLGS & zLGS): (a) for $L_1 = 10$, $L_2 = L_3 = 1$; (b) for $L_1 = 10$, $L_2 = 1$, $L_3 = 0.1$.

stretched grid cells occur. In [30] it was found that a plane smoother was a necessary tool when $L_1 > L_2 \sim L_3$ (test case 1) and $L_1 > L_2 > L_3$ (test case 2). These test cases are investigated with V(1,1) multigrid cycles, meaning V-cycles with 1 pre- and 1 postsmoothing iteration. In Fig. 5a the multigrid convergence results with (y,z)GS and yLGS followed by zLGS are presented for test case 1, choosing $L_1 = 10$, $L_2 = 1$, $L_3 = 1$ on a $49 \times 49 \times 49$ grid. GMRES stop criterion $\varepsilon = 10^{-8}$ is compared with other stop criteria, where the planes are solved with less accuracy, in order to see when the multigrid convergence rate of (y,z)GS with the high plane solution accuracy is obtained.

It is clear from Fig. 5a that a plane smoother is a necessary requirement; the convergence of the alternating line smoother is not satisfactory. Furthermore, the multigrid convergence behavior of (y,z)GS with GMRES criterion $\varepsilon = 10^{-1}$ is similar to the convergence with $\varepsilon = 10^{-8}$. With the other criterion $\varepsilon = 0.5$ extra multigrid iterations are needed to reduce the residual sufficiently.

In Fig. 5b the multigrid convergence for test case 2, choosing $L_1 = 10$, $L_2 = 1$, $L_3 = 0.1$ is presented on a $49 \times 49 \times 49$ grid. Also in this second test case the plane smoother is superior, especially while a relatively coarse grid is chosen. On finer grids the convergence rate of multigrid with the line smoother further increases toward 1, while the convergence of multigrid with plane smoothers does not change. With $\varepsilon = 10^{-1}$ three instead of two multigrid iterations are needed for the required convergence.

In Table 1 the average number of GMRES iterations per plane on all multigrid levels is presented for the stop criteria with satisfactory convergence behavior, $\varepsilon = 10^{-8}$ and $\varepsilon = 10^{-1}$. Also the number of iterations for $\varepsilon = 5.10^{-3}$ is shown, because with this criterion again only two multigrid iterations were needed in test case 2. It can be seen that with $\varepsilon = 10^{-1}$ and $\varepsilon = 5.10^{-3}$ many inner GMRES iterations are saved. Wall-clock times and the number of multigrid iterations needed are presented in Table II, where for comparison the time for several iterations of multigrid with the alternating line smoother is also shown. Instead of the linear correction scheme the same algorithmic environment as for the incompressible Navier–Stokes equations (FAS) is used, where the 3D matrix has not been stored, neither have the 2D matrices in the planes. FAS is only used here, because it is the solver developed for all equations considered. For linear equations, like the Poisson equation the algorithm produces the same results as the linear multigrid correction scheme. The times are obtained using two processors of an IBM SP2 computer, where the actual calculation took place on a ''wide'' node. The wall-clock time for test case 1 after six multigrid iterations with the line smoother is comparable to the time with (y,z)GS with $\varepsilon = 10^{-1}$. However, in six iterations the line smoother did not converge, as is shown in Fig. 5. The times of the line smoother are only presented for comparison with the time for the plane smoother, which solved the problem in six iterations. It is interesting to observe that for test case 2 the wall-clock time with the plane smoother is less than the time needed for two multigrid iterations with the line smoother.

4.2. *Incompressible Model Flow Problem*

As a 3D incompressible Navier–Stokes test problem the flow in a tube with rectangular cross section is investigated.

TABLE I

Average Number of Inner GMRES Iterations per Plane for Different Stop Criteria in (y,z)GS for the 3D Poisson Equation on a $49 \times 49 \times 49$ Stretched Grid

	Test case 1			Test case 2		
	ε			ε		
MG level	10^{-8}	10^{-1}	5.10^{-3}	10^{-8}	10^{-1}	5.10^{-3}
1 (=finest)	15.9	2.3	4.4	8.4	1.2	2.2
2	10.8	1.9	3.6	5.3	0.9	1.7
3	6.6	1.6	2.5	3.4	0.9	1.4
4	3.6	0.7	1.4	2.1	0.7	0.7

TABLE II

Wall-Clock Times (seconds) and Number of Multigrid Iterations for Different Stop Criteria in the Plane Smoother and for the Line Smoother for the 3D Poisson Equation on a 49 × 49 × 49 Stretched Grid

		Test case 1		Test case 2	
Smoother	Criteria	No. its.	Sol. time	No. its.	Sol. time
Plane	$\varepsilon = 10^{-8}$	6	150.0	2	32.4
	$\varepsilon = 10^{-1}$	6	109.9	3	39.1
	$\varepsilon = 5.10^{-3}$	6	115.2	2	27.4
Line	yLGS & zLGS (for time comparison)	6	103.4	2	35.7
				3	52.6

In the tube grids with severe stretching are generated. The domain from Fig. 4 is again taken for this test problem. Parameter L_1 in Fig. 4 is varied from 10 to 100, L_2 and L_3 are set to 1. The stretching is chosen in the flow direction, because that seems to be a natural choice for realistic flow problems around objects.

At inflow a fully developed inflow profile is prescribed; at outflow Neumann boundary conditions with a fixed pressure are given.

For different Reynolds numbers (Re) different underrelaxation factors are used in the plane Gauss–Seidel smoothers. Optimal values were found (as in [32]) to be

$$\begin{aligned} &\mathrm{Re} < 100 : \omega = 1.0; \quad 100 \le \mathrm{Re} < 1000 : \omega = 0.8; \\ &\mathrm{Re} \ge 1000 : \omega = 0.6. \end{aligned} \tag{17}$$

For the line smoothers the optimal underrelaxation factor appeared to be 1, independent of the Reynolds number. First, the first-order upwind discretization is solved to test the influence of the Reynolds number and the grid stretching on the multigrid algorithm. The solution method for first-order accuracy is the inner loop inside defect correction and therefore its convergence rate also influences the second-order convergence. The GMRES plane solver is more expensive with respect to wall-clock time and storage for this matrix resulting from a system of equations than for the Poisson equation. The matrix for a system of equations (four unknowns) must be stored for a 2D plane. Furthermore, for the truncated ILU preconditioner the same amount of storage is needed. Next to these two ''double precision'' arrays, seven smaller integer arrays with pointers to elements of the 2D plane matrix and the preconditioner are necessary.

Figure 6 presents the V(1,1)- and F(1,1)-cycle multigrid convergence for $L_1 = 100$ and Re = 1000. The convergence is shown for three grid sizes: Figure 6a 17^3 grid, Fig. 6b 33^3 grid, and Figure 6c 49^3 grid. Again the plane smoother (y,z)GS is compared to the alternating line smoother, yLGS & zLGS.

Level independent convergence rates are observed, comparing Figs. 6a, 6b, and 6c, which is typical for multigrid solution methods. Furthermore, it is found that the much cheaper algorithm with $\varepsilon = 10^{-1}$ produces similar convergence rates as the algorithm with $\varepsilon = 10^{-8}$. Also it can be seen that the rates with the plane smoother in the F-cycle are much better than the rates with the line smoother.

In Table III μ_{15} is shown for three Reynolds numbers, 10, 100, and 1000, to observe differences between diffusive dominance (Re $\le$ 100) and convective dominance (Re $\ge$ 1000) for the first-order discretization scheme. The grid considered consists of 49^3 grid points, and the grid stretching L_1 varies from 10 to 100. The F(1,1)-cycle is used with three smoothers, yLGS followed by zLGS, (y,z)-plane lexicographical Gauss–Seidel and (y,z)-plane zebra Gauss–Seidel. As the stop criterion for GMRES we chose $\varepsilon = 10^{-8}$; we would like to investigate whether a plane smoother is a necessary requirement and, therefore, the plane is solved in every smoothing iteration with high accuracy.

In Table III it can be seen that the plane smoothers are superior over the alternating line smoother, when the grid stretching is more than a factor 10. This is especially true for lower Reynolds numbers. For $L_1 = 10$ the behavior of all smoothers is still comparable for higher Reynolds numbers. It can be observed that the zebra plane smoother produces better convergence rates than the lexicographical plane smoother for the low Reynolds case Re = 10. For the other cases the results of the zebra and lexicographical plane Gauss–Seidel smoothers are comparable. Finally, from Table III it is expected that with a larger stretching the need for the plane smoothers will be even more pronounced.

Defect Correction. It is now interesting to compare the convergence behavior for the defect correction technique with the results obtained above. The channel flow problem with parameters $L_1 = 100$, $L_2 = L_3 = 1$, and Re = 1000 is again chosen. The combination of defect corrections with (y,z)GS appeared to converge optimal with a V(1,1)-cycle as inner iteration. An F-cycle did not lead to further convergence acceleration.

Figure 7 presents the defect correction convergence behavior for different GMRES stop criteria within (y,z)GS on a 33^3 grid. They are compared with the line smoother in F(1,1) that showed satisfactory convergence rates for the first-order accurate discretization (Figure 6 and Table III). In Fig. 7 it can be seen that the convergence for stop

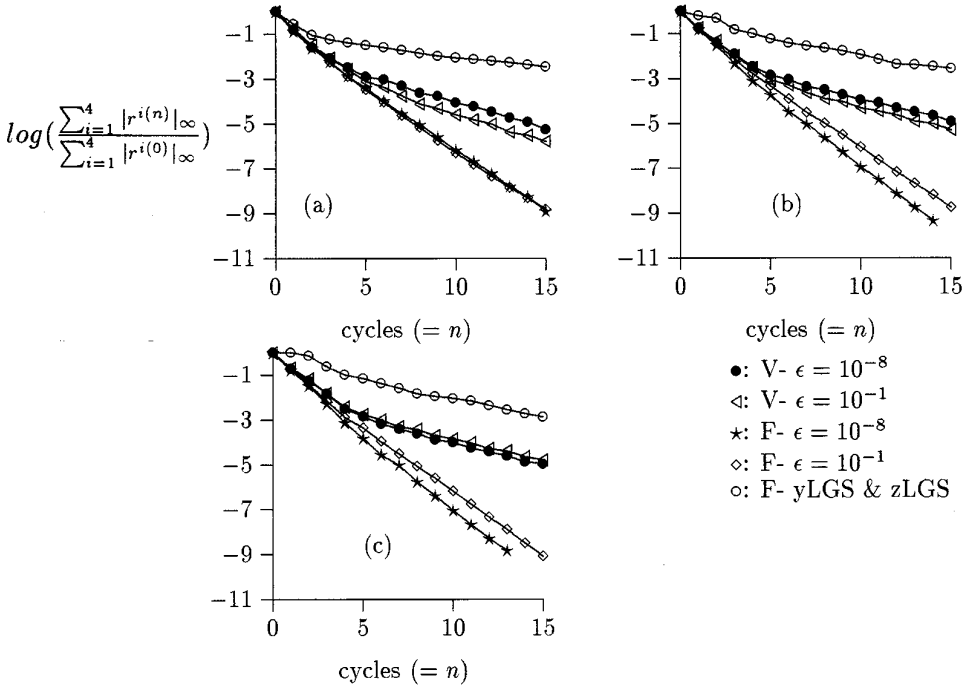

FIG. 6. V- and F-cycle multigrid convergence for 3D inc. Navier–Stokes equations (Re = 1000). (y,z)GS with two stop criteria for GMRES is compared with yLGS & zLGS, for $L_1 = 100$, $L_2 = L_3 = 1$: (a) 17^3-grid; (b) 33^3-grid; (c) 49^3-grid.

criterion $\varepsilon = 10^{-2}$ is identical with $\varepsilon = 10^{-6}$. The other criteria produce a slightly worse convergence behavior. The algorithm with the line smoother converges slowly; μ_{20} is 0.83. Furthermore, it was found that the algorithm with the zebra plane smoother did not lead to satisfactory results for the second-order discretization.

Table IV compares the average number of GMRES iterations per plane for criteria $\varepsilon = 10^{-1}$, $\varepsilon = 10^{-2}$, and $\varepsilon = 10^{-6}$. This average number is presented for 20 multigrid defect correction iterations for all multigrid levels, except for the coarsest (=level 4 for the 17^3 grid and level 5 else). Also, the average reduction factor μ_{20} is shown for (y,z)GS in Table IV.

Table IV shows that with $\varepsilon = 10^{-2}$ many GMRES iterations are saved compared to $\varepsilon = 10^{-6}$ and that the multigrid

TABLE III

Single Block Convergence Rates for Line and Plane Smoothers on a 49^3 Grid with Different Stretching of Grid Cells (L_1) in x-Direction and for Reynolds Numbers 10, 100, and 1000

Re	Smoother	$L_1 = 10$	$L_1 = 20$	$L_1 = 50$	$L_1 = 100$
10	yLGS & zLGS	0.65	0.80	0.86	0.94
	(y,z)GS	0.24	0.35	0.56	0.62
	(y,z)ZGS	0.27	0.25	0.22	0.42
100	yLGS & zLGS	0.44	0.56	0.70	0.86
	(y,z)GS	0.44	0.24	0.20	0.22
	(y,z)ZGS	0.29	0.28	0.25	0.20
1000	yLGS & zLGS	0.40	0.43	0.50	0.69
	(y,z)GS	0.31	0.24	0.22	0.20
	(y,z)ZGS	0.43	0.26	0.22	0.22

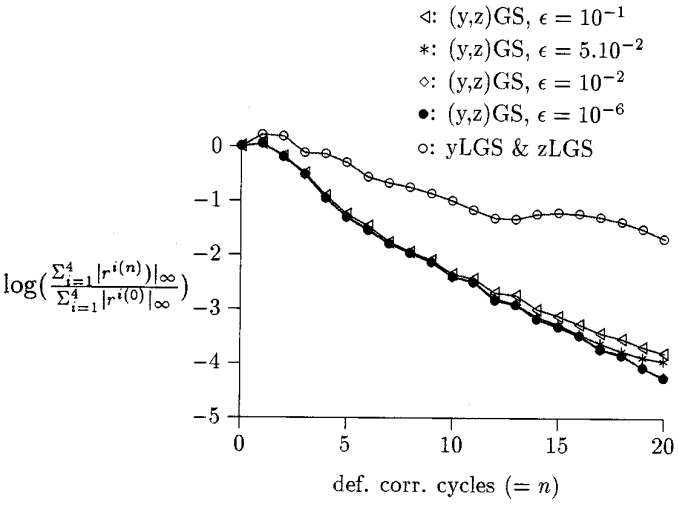

FIG. 7. Convergence of second-order residuals compared for different stop criteria ε in GMRES for a 3D incompressible channel problem at Re = 1000, stretching parameters: $L_1 = 100$, $L_2 = L_3 = 1$; 33^3 grid points.

TABLE IV

Average Number of GMRES Iterations per Multigrid Level (20 mg-iterations) and Defect Correction Convergence Rates μ_{20} for V(1,1) and (y,z)GS with Different Stop Criteria Stretching $L_1 = 100$ and Re = 1000

		# GMRES its. on mg. level				
Grid	ε	1 (=finest)	2	3	4	μ_{20}
17^3	10^{-1}	8.2	5.7	3.7	—	0.65
	10^{-2}	11.5	8.5	5.2	—	0.63
	10^{-6}	23.8	16.5	10.7	—	0.63
33^3	10^{-1}	9.1	7.7	5.7	4.2	0.65
	10^{-2}	15.9	11.8	8.7	6.0	0.61
	10^{-6}	33.9	23.8	16.4	10.7	0.61
49^3	10^{-1}	10.7	8.9	7.4	4.8	0.63
	10^{-2}	18.5	14.1	10.5	7.2	0.62
	10^{-6}	41.0	29.2	20.1	13.8	0.62

convergence is not influenced on all grids investigated. With $\varepsilon = 10^{-1}$ the multigrid convergence is also very satisfactory on the 49^3 grid. The average reduction factor μ_{20} for yLGS+zLGS in F(1,1) was 0.83 on the three grids considered. Table V compares wall-clock times for 20 defect correction iterations of (y,z)GS with $\varepsilon = 10^{-2}$ and of yLGS+zLGS. The differences in wall-clock timers can clearly be observed.

Discussion. It is interesting to see that it is not necessary to solve equations for a plane exactly in a plane smoother. Even though, it is not guaranteed that the fixed stop criterion, $\varepsilon = 10^{-2}$, found will work for all problems to be considered in the future. A robust generalization of the stop criterion for software implementations will be an adaptive stop criterion, for example, depending on the current residual in a plane. This is the right-hand side in the smoother, as can be seen in (13). It means that the criterion is being made smaller during multigrid iterations;

TABLE V

Wall-Clock Times (seconds) for 20 V(1,1) Defect Correction Iterations for (y,z)GS with Stop Criterion $\varepsilon = 10^{-2}$ and for yLGS & zLGS in F(1,1) for a 3D Stretched Incompressible Channel Problem

	Grid		
Smoother	17^3	33^3	49^3
(y,z)GS, $\varepsilon = 10^{-2}$	330	3339	13331
yLGS & zLGS	294	2447	10167

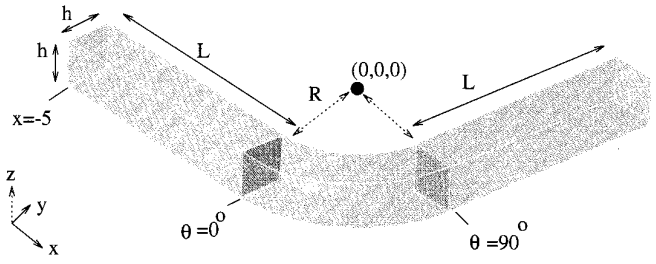

FIG. 8. Domain for flow over a 3D square duct with a 90° bend, and division into three blocks.

after some iterations planes are being solved with higher accuracy.

Instead of using a plane smoother in standard multigrid for solving these anisotropic problems, which is considered as an expensive algorithm, research has started to use nonstandard multilevel algorithms [11, 15, 17], where a coarse grid correction is made more robust, so that a cheaper smoother can be used. Our convergence and timing results can be taken as starting point for comparison with such nonstandard multigrid algorithms for 3D CFD problems.

4.3. *Three-Dimensional Flow in a 90° Bending Square Duct*

The problem studied here is the 3D channel flow problem in a 90° bending square duct. Several researchers used the geometry presented in Fig. 8 with $L = 5$ to solve the flow problem at Re = 790 (see [18] and the references therein). A fully developed inflow velocity profile is imposed at the inlet boundary; at the outflow boundary Neumann boundary conditions are prescribed.

We use this flow problem to study the influence of parameter L on the defect correction convergence. The Reynolds number, based on the mean entrance velocity and the duct width is assumed to be 100. L varies from 20 to 100; $h = 1$; $R = 1.8$. The flow domain is split into three blocks, consisting of $33 \times 33 \times 33$ points, as is depicted in Fig. 8. Again the lexicographical plane smoother with GMRES stop criterion $\varepsilon = 10^{-2}$ is compared to the alternating line smoother. The defect correction convergence of the second-order results with multigrid F(2,2)-cycles is presented in Fig. 9 for $L = 20$, $L = 50$, and $L = 100$. Figure 9 shows that for $L \geq 50$ the plane smoother is beneficial. For $L = 20$ also the alternating line smoother presents a satisfactory convergence. It is interesting to observe that the convergence is not really influenced by the large discontinuity in stretching at the block boundaries for $L = 100$. For this three-block problem the differences in wall-clock time between the plane and the alternating line smoother are more pronounced: 20 F(2,2) defect correction cycles with yLGS and zLGS cost 3340 s, 20 F(2,2)

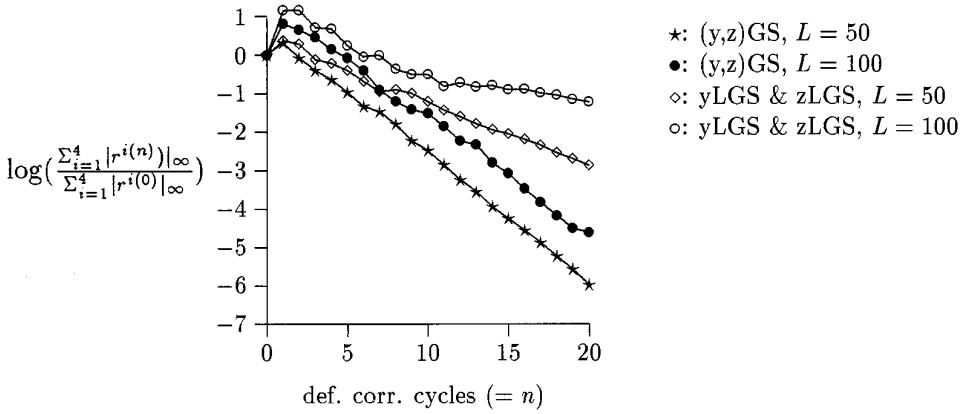

FIG. 9. Comparison of F(2,2) convergence of defect correction between (y,z)GS and yLGS+zLGS, flow in a 3D duct at Re = 100 for different values of parameter L.

cycles with the plane smoother cost 5700 s on 4 IBM SP2 thin nodes.

Finally, Fig. 10 shows the vector field with reduced resolution in the mid-span plane in the curve for the flow at Re = 100.

4.4. *Laminar Backward-Facing Step Flow*

In order to test flow problems with stretching in two directions ($L_1 > L_2 > L_3$) we choose here, instead of the systemic approach of Subsection 4.2, to investigate one test problem, the laminar flow over a backward-facing step. This well-known channel flow is well studied for 2D discretizations (for example, in [12, 31]). For the 2D flow experimental results are known [2], obtained in a 3D test section. The configuration is shown in Fig. 11. It is split into four blocks here for parallel solution.

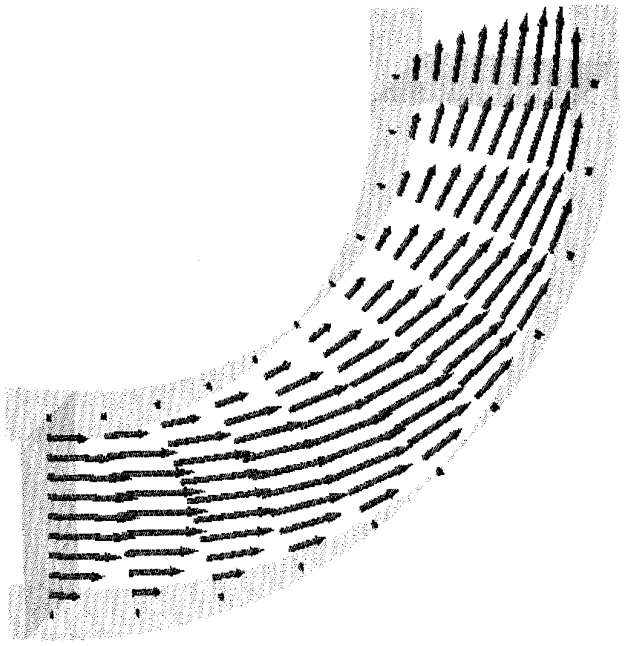

FIG. 10. Vector field (reduced resolution) in the mid-span plane for flow over a 3D square duct with a 90° bend, Re = 100.

A result of interest for this problem is, for example, the length of the first recirculation zone. The 2D computational results agree with the experiments only for a certain range of Reynolds numbers, up to Re = 400. For higher Reynolds numbers the computed recirculation lengths are too small [12, 31], due to 3D effects. We try to find the recirculation lengths found with the experiments by solving the 3D incompressible Navier–Stokes equations in a wide backward-facing step channel. The geometrical parameters in Fig. 11 are chosen as $h_1 = 72$, $h_2 = 4$, $h_3 = 1$, $H = 2$ for all Reynolds numbers.

In blocks 2, 3, and 4 with parameters $L_1 = 24$, $L_2 = 4$, $L_3 = 2$ stretched grids with $17 \times 33 \times 49$ points per block are generated. These parameters are especially chosen, so that grid stretching occurs in two directions, and the problems need to be solved with a plane smoother. In block 1 $17 \times 33 \times 25$ grid points are generated, which means a load-imbalance among the blocks. However, that is of no concern in this test. The computations presented are for Reynolds in the range between 400 and 1000 with the Reynolds number defined as in [2], Re = $\overline{U}.H/\nu$. $\overline{U}$ is the average velocity, which is for large values of h_2 approximately equal to two-thirds of the maximum inlet velocity.

At the outflow boundary Neumann boundary conditions are prescribed; at inflow a fully developed inflow is given.

For the first-order discretization the alternating line and the (y,z)GS smoother were converging with similar rates ($\mu_{20} \approx 0.45$ for F(1,1) for all Reynolds numbers investigated). However, for the defect correction it was found

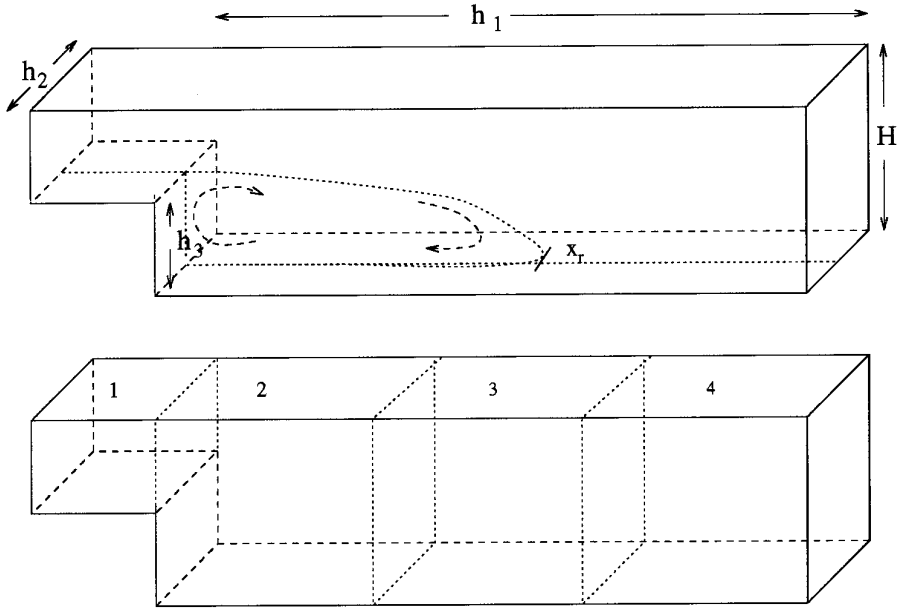

FIG. 11. Domain for flow over a 3D backward-facing step and division into four blocks.

that the alternating line smoother produced satisfactory results only until Re = 600 (μ_{50} = 0.79 for Re = 300), (y,z)GS produced satisfactory convergence rates for all Reynolds numbers investigated (μ_{50} = 0.76 for Re = 400; μ_{100} = 0.83 for Re = 800).

The length of the first recirculation zone (x_r) after the step is determined on the center line of the channel. This length is presented in Fig. 12. It is compared with the experimental results from [2] and with the 2D results from [31]. Figure 12 shows that the 2D computational results

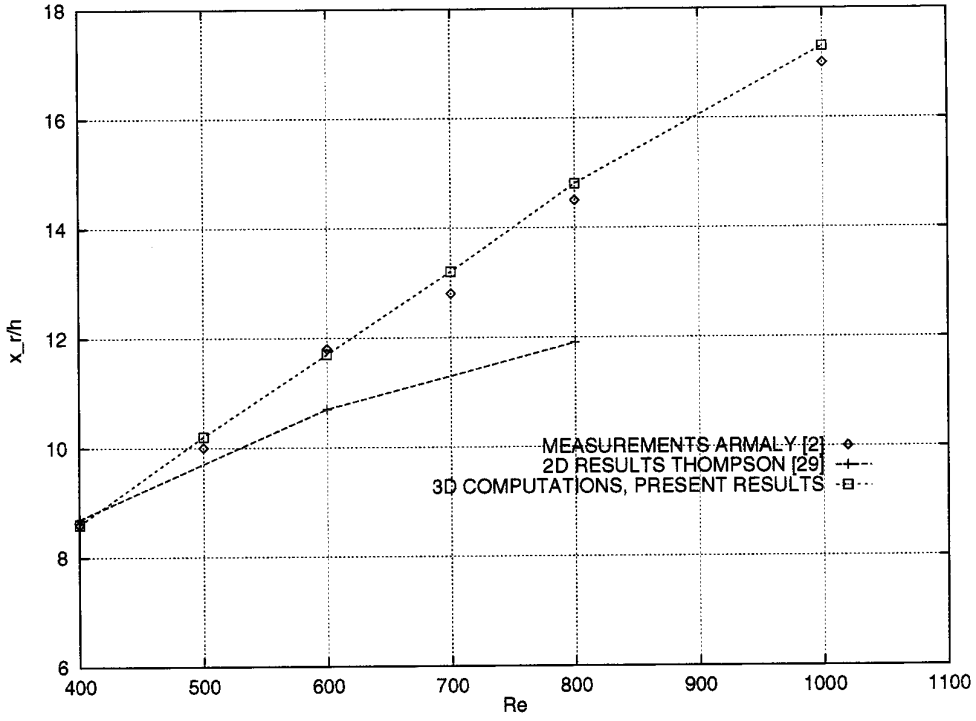

FIG. 12. The recirculation length found with the 3D method compared with measurements and 2D results.

from other papers deviate from the measurements. The length found in 2D flow experiments in [2] is in very good agreement with the results from Fig. 12, which confirms the statement that a 3D flow is generated in the experiments.

5. CONCLUSIONS

A multigrid algorithm to solve 3D problems with severely stretched grid cells has been presented. These problems with strongly coupled unknowns are solved with a plane smoother. A matrix is set up for all unknowns in a plane. It is solved iteratively with a preconditioned GMRES method. A stop criterion is tested which reduces the number of GMRES iterations and does not influence the multigrid convergence rate. It is found that the algorithm is very efficient for stretched Poisson problems. The algorithm produced good results when the GMRES plane solver was stopped after the initial residuals are diminished by a factor of 10. For the method with the plane smoother similar wall-clock times are obtained as for an alternating line smoother, while the convergence with the line smoother was not satisfactory for the Poisson problem considered.

The solution method has also been tested for 3D incompressible Navier–Stokes equations. The discretization is based on a flux splitting formulation of the equations and a collocated grid arrangement of primitive variables. For grid stretching in one direction the plane smoother was beneficial for cell aspect ratios of more than a factor of 50 for several flow problems at different Reynolds numbers. Here, the defect correction algorithm with the GMRES plane solver produced identical results as an ''exact''plane solver, when the GMRES iterations were stopped after the initial residuals were diminished by a factor of 100. Although a zebra plane smoother produced satisfactory multigrid convergence results for first-order accurate incompressible flow problems, the convergence within the defect correction was not as good as for the lexicographical plane smoother. For the backward-facing step problem, where the grid stretching was made such that a plane smoother was necessary for convergence the defect correction convergence rates increase. The computed recirculation lengths in a wide backward-facing step channel resembled the experimental results very well.

REFERENCES

1. Ch. Arakawa, A. Demuren, W. Rodi, and B. Schönung, ''Application of Multigrid Methods for the Coupled and Decoupled Solution of the Incompressible Navier–Stokes Equations,'' *Proceedings, 7th GAMM Conf. on Numer. Methods in Fluid Mech*., edited by M. Deville, Notes on Numer. Fluid Mech., Vol. 20 (Vieweg, Braunschweig, 1988), p. 1.
2. B. F. Armaly, F. Durst, J. C. F. Pereira, and B. Schönung, *J. Fluid Mech.* **127,** 473 (1983).
3. A. Behie and P. A. Forsyth Jr., *Appl. Math. Comput.* **13,** 229 (1983).
4. A. Brandt and N. Dinar, ''Multigrid Solutions to Flow Problems,'' in *Numerical Methods for Partial Differential Equations*, edited by S. Parter (Academic Press, New York, 1979), p. 53.
5. P. N. Brown and Y. Saad, *SIAM J. Sci. Stat. Comp.* **11,** 450 (1990).
6. R. Calkin, R. Hempel, H. C. Hoppe, and P. Wypior, *Parallel Comput.* **20,** 615 (1994).
7. E. Dick and J. Linden, *Int. J. Num. Methods Fluids* **14,** 1311 (1992).
8. W. S. Edwards, L. S. Tuckerman, R. A. Friesner, and D. C. Sorensen, *J. Comput. Phys.* **110,** 82 (1994).
9. B. Eisfeld, H-M. Bleecke, N. Kroll, and H. Ritzdorf, ''Structured Grid Solvers II, Parallelization of Block Structured Flow Solvers,'' in *Parallel Computing on Computational Fluid Dynamics*, VKI Lecture Series, Von Karman Inst., Rhode Saint Genèse Belgium, 1995.
10. U. Gärtel, A. Krechel, A. Niestegge, and H.-J. Plum, ''Parallel Multigrid Solution of 2D and 3D Anisotropic Elliptic Equations: Standard and Nonstandard Smoothing, in *Multigrid Methods III*, edited by W. Hackbusch and U. Trottenberg, Int. Ser. of Num. Math., Vol. 98 (Birkhäuser, Basel, 1991), p. 191.
11. W. Hackbusch, *Numer. Math.* **56,** 229 (1989).
12. J. Kim and P. Moin, *J. Comput. Phys.* **59,** 308 (1985).
13. B. Koren, *J. Comput. Phys.* **87,** 25 (1990).
14. J. Linden, B. Steckel, and K. Stüben, *Parallel Comput.* **7,** 461 (1988).
15. W. A. Mulder, *J. Comput. Phys.* **83,** 303 (1989).
16. C. W. Oosterlee, Ph.D. thesis, University of Delft, 1993 (unpublished).
17. C. W. Oosterlee, *Appl. Num. Math.* **19,** 115 (1995).
18. C. W. Oosterlee and H. Ritzdorf, *Int. J. Numer. Methods Fluids* **23,** 347 (1996).
19. S. V. Patankar, *Numerical Heat Transfer and Fluid Flow* (McGraw-Hill, New York, 1980).
20. M. Peric, Ph.D. thesis, University of London, 1985.
21. R. Reyret and T. D. Taylor, *Computational Methods for Fluid Flow* (Springer-Verlag, Berlin, 1983), p. 108.
22. A. van der Ploeg, Ph.D. thesis, University of Groningen (RUG), 1994 (unpublished).
23. D. Rayner, *Int. J. Num. Methods Fluids* **13,** 507 (1991).
24. C. M. Rhie and W. L. Chow, *AIAA J.* **21,** 1525 (1983).
25. H. Ritzdorf, A. Schüller, B. Steckel, and K. Stüben, *Parallel Comput.* **20,** 1559 (1994).
26. H. Ritzdorf, *CLIC—The Communications Library for Industrial Codes,* User's Reference Manual (GMD, Sankt Augustin, Germany, 1995).
27. Y. Saad and M. H. Schultz, *SIAM J. Sci. Stat. Comput.* **7,** 856 (1986).
28. Y. Saad, ''Preconditioned Krylov subspace methods for CFD Application,'' in *Proceedings, Int. Workshop on Solution Techniques for Large-Scale CFD Problems*, edited by W. G. Habashi (Cerca, Montréal/Québec, 1994).
29. P. Sonneveld, *SIAM J. Sci. Stat. Comput.* **10,** 36 (1989).
30. C. A. Thole and U. Trottenberg, *Appl. Math. Comput.* **19,** 333 (1986).
31. M. C. Thompson and J. H. Ferziger, *J. Comput. Phys.* **82,** 94 (1989).
32. S. P. Vanka, *Comput. Methods Appl. Mech. Eng.* **59,** 321 (1986).
33. B. van Leer, ''Upwind-Difference Methods for Aerodynamic Problems Governed by the Euler Equations, in *Large Scale Computations*

in Fluid Mechanics, edited by B. Enquist *et al.* Lectures in Applied Mathematics, Vol. 22, Amer. Math. Soc. Providence, 1985, p. 327.

34. C. Vuik, *Int. J. Numer. Methods in Fluids* **16,** 507 (1993).
35. P. Wesseling, *An Introduction to Multigrid Methods* (Wiley, Chichester, 1992).
36. G. Wittum, *Numer. Math.* **54,** 543 (1989).
37. S. Zeng and P. Wesseling, *Int. J. Numer. Methods Fluids* **20,** 59 (1995).
38. S. Zeng, C. Vuik, and P. Wesseling, ''Krylov Subspace and Multigrid Methods Applied to the Incompressible Navier–Stokes Equations,'' in *Proceedings, Copper Mountain Conf. 1995*, NASA Conference Publ., 1995.